applied sciences

MDPI

Article

Design and Synthesis of 3D-Graphene@C/Co@N-C Composites with Broadband Microwave Absorption Performance

Songyan Li, Xiaoxia Tian *, Jiafu Wang and Shaobo Qu

Shaanxi Key Laboratory of Artificially-Structured Functional Materials and Devices, Air Force Engineering University, Xi'an 710051, China

* Correspondence: xiaoxiatian@126.com

Abstract: Improving the microwave absorption performance of Co-MOF-derived Co@N-C composite by constructing the morphology and spatial structure is a known challenge. In this work, under the action of the binder polyvinylpyrrolidone, 3D-graphene particles can be well decorated on the surface of the Co@N-C composite after high-temperature pyrolysis. In addition, due to the structural characteristics of MOFs, Co particles can be well covered by a carbon layer, which effectively solves the problem that magnetic metal particles are prone to corrosion and oxidation. The microwave absorption performances of the composite can be well adjusted by changing the average dotted density of the 3D-graphene on the Co@N-C composite. It is worth noting that the maximum reflection loss can reach −58.72 dB at the thickness of 1.64 mm, and the maximum effective absorption bandwidth can achieve 5.74 GHz at the 1.79 mm thickness, which almost covers the whole Ku band. Importantly, these results demonstrate that 3D-graphene@C/Co@N-C composites have great potential as high-efficiency microwave absorption materials.

Keywords: 3D-graphene@C/Co@N-C; microwave absorption; double-loss mechanism; impedance matching

Citation: Li, S.; Tian, X.; Wang, J.; Qu, S. Design and Synthesis of 3D-Graphene@C/Co@N-C Composites with Broadband Microwave Absorption Performance. *Appl. Sci.* **2022**, *12*, 9390. https://doi.org/10.3390/app12189390

Academic Editor: Antonio Di Bartolomeo

Received: 11 July 2022
Accepted: 17 September 2022
Published: 19 September 2022

1. Introduction

With the large-scale application of electronic devices, electromagnetic interference and electromagnetic pollution have become a major problem [1]. Nowadays, some researchers have developed the mixture of microwave absorption materials and paraffin to absorb microwaves in specific frequencies, and the research in this field is developing towards a low filling rate, ultra-thin, broadband, and strong absorption [2–4].

Metal-organic frameworks (MOFs) are skeletal crystalline materials composed of metal ions and organic ligands. Under the action of high-temperature pyrolysis, the carbon in the organic ligands is converted to elemental carbon, and the metal ions are reduced to metal elements or metal oxides [5]. Some studies found that MOFs derived composites with a double-loss mechanism have great application prospects in the field of microwave absorption, for example, Co/Ni-MOFs-derived porous and hollow CoNi@C microspheres [6], Co-MOF@Zn-MOF-derived Co-C@C hollow composites [7], acidified bimetallic MOFs constructed Co/N codoped low-dimensional hybrid carbon networks [8]. However, due to the limitation of the type of organic ligand, the electrical loss of some MOF-derived composites is relatively poor, which will affect their microwave absorption performances. It is worth noting that some researchers have found that the inherent defects of MOFs can be overcome by combining MOFs with carbon material and reasonably designing the morphology and spatial structure of the composite, for example, the multicavity-structured MOF derivative/porous graphene hybrid [9], the in situ-derived carbon nanotube-decorated nitrogen-doped carbon-coated nickel hybrids from MOF/melamine [10], and the Co/ZnO/C@MWCNTs based on carbon nanotube-coated MOFs [11].

Inspired by the above research, and in order to improve the microwave absorption performance of Co-MOF-derived Co@N-C composites, 3D-graphene@C/Co@N-C composites were prepared by high-temperature pyrolysis. Compared with other graphene composites, the synthesis method of the 3D-graphene@C/Co@N-C composite is relatively convenient, which provides a reference for large-scale preparation [12–15]. By constantly adjusting the ratio of raw materials, the composite obtained excellent microwave absorption performances in the Ku band. Importantly, the research results of this work can be applied to a wide range of scenarios. For example, the mixture of composite and paraffin can act not only as the sandwich material for a wave-permeable device to block the transmission of the Ku band microwave, but also as the coating material of the wall of the room where precision instruments are stored to absorb Ku-band clutter in the room.

2. Experimental Section

2.1. Materials

The 2-methylimidazole ($C_4H_6N_2$) and ethanol were purchased from Sinopharm Chemical Reagent Co., Ltd. (Shanghai, China). Cobalt nitrate hexahydrate ($Co(NO_3)_2 \cdot 6H_2O$) was purchased from Chengdu Cologne Chemical Co., Ltd. (Chengdu, China). Polyvinylpyrrolidone (PVP-K30) was purchased from Tianjin Kemiou Chemical Reagent Co., Ltd. (Tianjin, China). The 3D-graphene prepared by chemical vapor deposition was purchased from Changzhou Carbon Glory New Material Co., Ltd. (Changzhou, China). Deionized water was prepared by pure water machine.

2.2. Synthesis of Co-MOF

The Co-MOF was prepared by a simple chemical reaction. First, 0.096 mol $C_4H_6N_2$ was dissolved in 100 mL deionized water and named solution A. Then, 0.02 mol $Co(NO_3)_2 \cdot 6H_2O$ was dissolved in 50 mL deionized water and named solution B. After that, solution B was slowly added to solution A and stirred continuously at room temperature for 2 h. Finally, the collected products were washed with deionized water to remove the excess ions, and dried at 80 degrees Celsius for 2 h in an electric blast drying oven to obtain Co-MOF.

2.3. Synthesis of 3D-Graphene@C/Co@N-C Composites

The 3D-graphene@C/Co@N-C composites were prepared by high-temperature pyrolysis. First, 0.40 g Co-MOF and 0.30 g PVP-K30 were added to 30 mL ethanol and stirred at room temperature for 30 min, and named solution C. Then, 3D-graphene (0.10 g, 0.20 g, 0.30 g) was added to solution C and stirred continuously at 80 degrees Celsius until the ethanol evaporated. Finally, the collected mixtures were ground into powder and placed in a tubular furnace and calcined at 600 degrees Celsius for 2 h at the heating rate of 5 degrees Celsius/min, and the whole process was protected by argon. The three groups of composites were successively labeled as CNCG-1, CNCG-2, and CNCG-3. As a control, a Co@N-C composite was prepared by the same method and labeled as CNC.

2.4. Characterizations

The morphology and structure were characterized by scanning electron microscope (SEM, S-4800) and transmission electron microscope (TEM, JEM-2100). An X-ray diffraction (XRD, D8 Advance) was used for the phase structure analysis, and the test range was 10–80° with a sampling step of 0.02°. Raman spectrum (Raman, DXRxi) was used for graphization degree analysis, and the laser wavelength was 532 nm, the grating was 1800 L/mm, and the line resolution was 1.6 nm/mm. The X-ray photoelectron spectra (XPS, AXIS SUPRA) were used for the chemical composition and functional group binding analysis. Magnetic properties were measured by the vibrating sample magnetometer (VSM, Model 7400 series), and the magnetic field strength was 2 T. To evaluate the microwave absorption performances of the composite, the mixture containing 15% composite and 85% paraffin was pressed into a coaxial ting with inner diameter of 3.04 mm and outer diameter of 7.00 mm in a mold, and its electromagnetic parameters in the 2–18 GHz range were

measured using the vector network analyzer (VNA, N5224A). According to transmission line theory, the reflection loss (RL) can be calculated by the following equations [16]:

$$Z_{in} = Z_0(\mu_r/\varepsilon_r)^{1/2} \tan h\left[j2\pi fd/c(\mu_r\varepsilon_r)^{1/2}\right] \quad (1)$$

$$RL = 20\lg|(Z_{in} - Z_0)/(Z_{in} + Z_0)| \quad (2)$$

where Z_0 is the impedance of free space and Z_{in} is the normalized input impedance, respectively, ε_r and μ_r are, respectively, the complex permittivity and permeability, f is the frequency of the incident wave, d is the thickness of the sample, and c is the speed of light in free space.

3. Results and Discussion

Figure 1 shows the SEM images of all composites. The Co-MOF-derived CNC has the sheet structure in general (Figure 1a). As shown in Figure 1b–d, under the action of the binder PVP-K30, the 3D-graphene particles can be well dotted on the surface of the CNC after the high-temperature pyrolysis. In addition, it can be observed that the average dotted density of the 3D-graphene on the CNC was positively correlated with the additive amount of the 3D-graphene. Compared with the CNCG-1 and CNCG-3, CNCG-2 has the best morphology and spatial structure. Figure 2 shows the HR-TEM image of the CNC. The lattice fringe with the spacing of 0.21 nm corresponds with the (111) plane of the Co crystal, and the lattice fringe with the spacing of 0.35 nm corresponds with the graphite carbon.

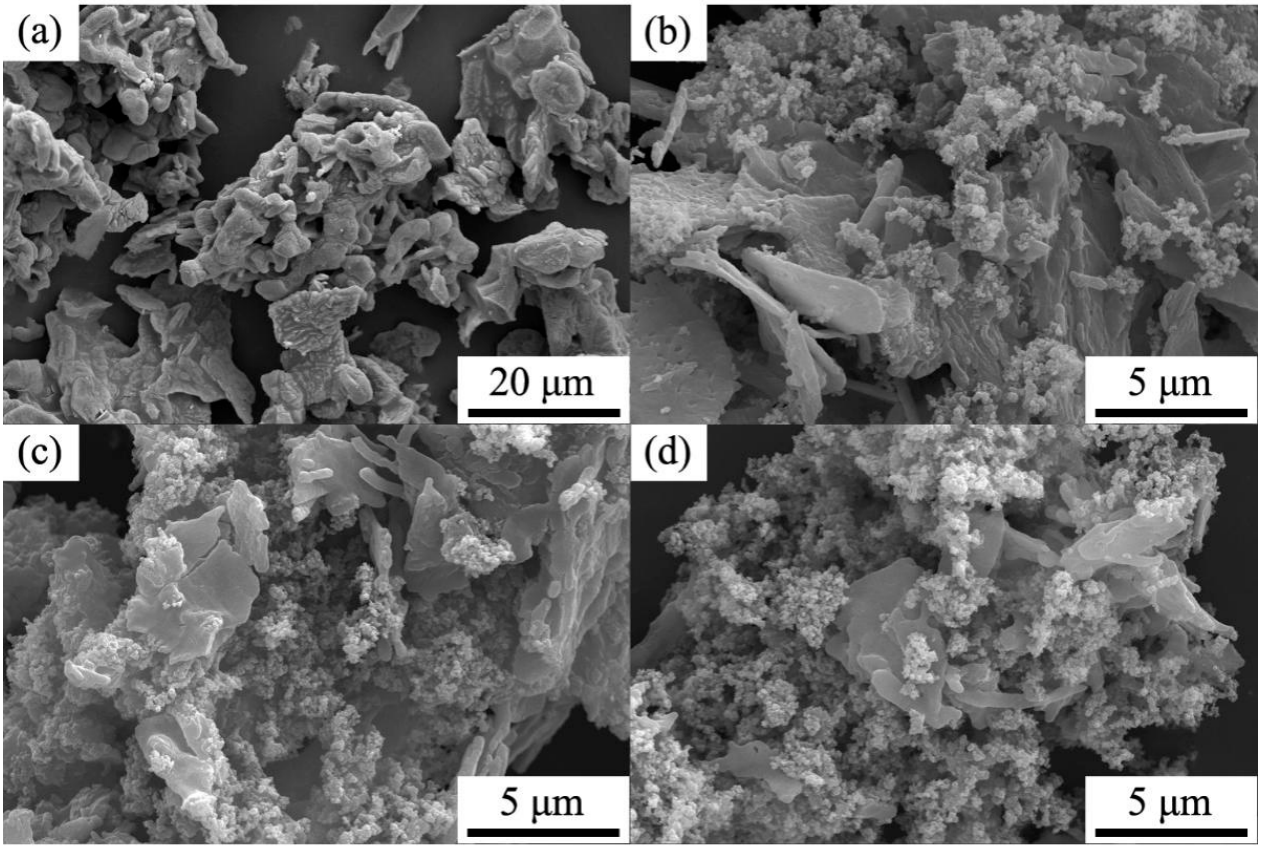

Figure 1. The SEM images of all composites. (**a**) The SEM image of CNC; (**b**) The SEM image of CNCG-1; (**c**) The SEM image of CNCG-2; (**d**) The SEM image of CNCG-3.

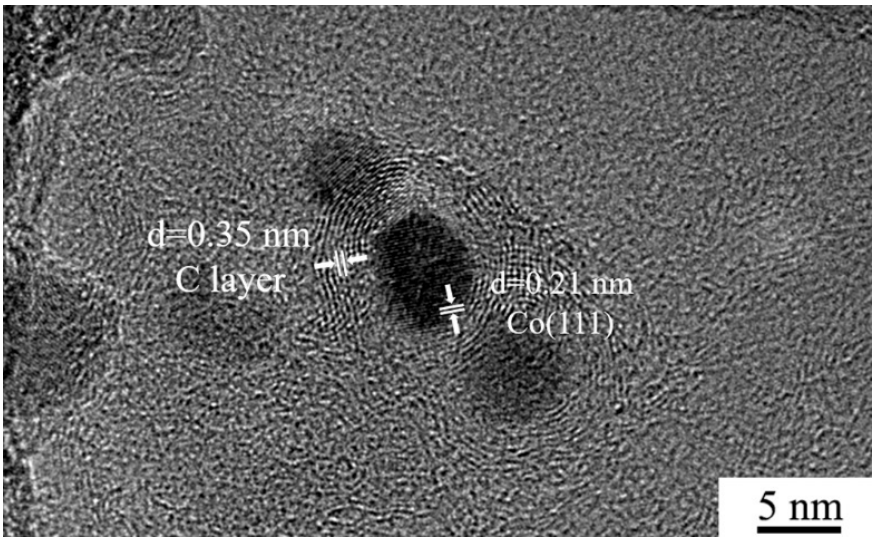

Figure 2. The HR-TEM image of CNC.

The crystal structures of all composites were studied by XRD patterns (Figure 3a). There is an obvious characteristic peak around 26°, which is derived from the response of the (002) plane of carbon (JCPDS no. 41-1487). In addition, the three diffraction peaks at 44.16°, 51.40°, and 75.84° correspond to the (111), (200), and (220) crystal planes of Co (JCPDS: 15-0806), indicating that Co^{2+} was successfully reduced to Co under the action of carbon. The states of carbon in all composites were studied by Raman spectroscopy (Figure 3b). The two characteristic bands at 1350 and 1580 cm^{-1} correspond to the D band and G band, which are attributed to the lattice defects of the carbon atom and the in-plane vibration of the sp2 carbon atom, respectively. The intensity ratios of the D band to G band (I_D/I_G) can be used to judge the graphitization degree of the carbon-containing composites. The I_D/I_G of all composites are 0.850, 0.905, 1.075, and 1.107, respectively. The magnetic properties of all composites were studied by VSM (Figure 4). The saturation magnetization (Ms) of all composites was 33.63, 18.99, 15.97, and 13.81 emu/g, respectively, all of which show the ferromagnetic behavior. In addition, it is obvious that the CNC has the highest Ms, mainly because the carbon content of the CNC is relatively low.

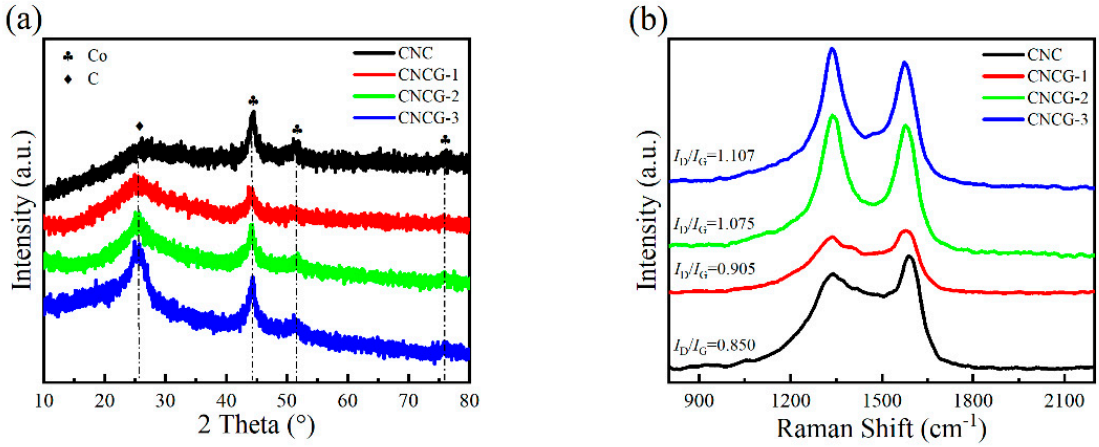

Figure 3. The XRD patterns and Raman spectra of all composites. (**a**) The XRD patterns of all composites; (**b**) The Raman spectra of all composites.

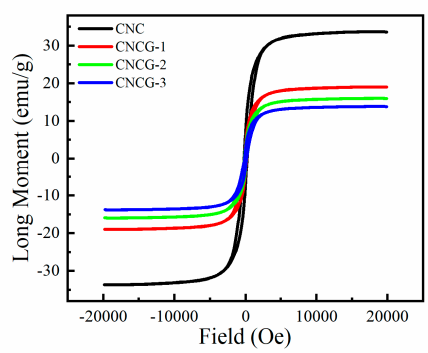

Figure 4. The room-temperature hysteresis loops of all composites.

The surface chemical composition and states of the CNCG-2 were studied by XPS. The XPS spectrum of CNCG-2 demonstrates the existence of Co, C, O, and N elements (Figure 5a). The fitting peak of Co 2p at 778.47 eV indicates that the existence of Co atom (Figure 5b). The two fitting peaks of C 1s at the binding energies of 284.74 and 285.42 eV are related to C-C/C=C and C-O groups (Figure 5c), respectively. The two fitting peaks of N 1s at binding energies of 398.99 and 400.77 eV are directly related to pyridine nitrogen and pyrrole nitrogen (Figure 5d). Oxygen-containing functional groups, pyridine nitrogen, and pyrrole nitrogen can act as polarization centers to enhance the intensity of dipole polarization [10].

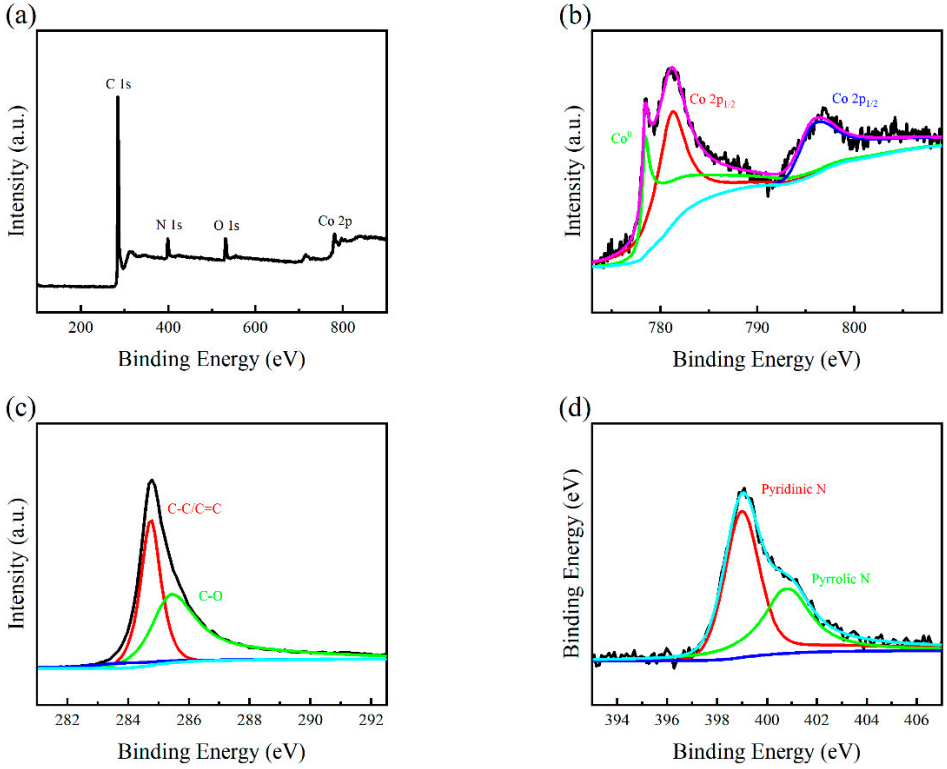

Figure 5. The Raman spectra of CNCG-2. (**a**) The XPS spectrum of CNCG-2; (**b**) The Co 2p spectrum of CNCG-2; (**c**) The C 1s spectrum of CNCG-2; (**d**) The N 1s spectrum of CNCG-2.

The microwave absorption capacity of the material is determined by its electromagnetic parameters, including complex permittivity ($\varepsilon_r = \varepsilon' - j\varepsilon''$) and complex permeability ($\mu_r = \mu' - j\mu''$). Generally speaking, the ε' and μ' represent the storage capacity of the electrical energy and the magnetic energy, while the ε'' and μ'' represent the loss capacity of the electrical energy and the magnetic energy. In addition, the dielectric loss tangent ($\tan \delta_\varepsilon = \varepsilon'' / \varepsilon'$) and the magnetic loss tangent ($\tan \delta_\mu = \mu'' / \mu'$) can be used to describe the dielectric loss capacity and the magnetic loss capacity [17]. Compared with the CNC, the

values of ε_r of CNCG significantly enhance in the frequency range of 2–18 GHz (Figure 6a,b). Due to the introduction of appropriate amount of the 3D-graphene, the values of ε_r of CNCG-2 are obviously better than that of the other composites. As the frequency changes from 2 to 18 GHz, the values of μ_r of all composites have the same variation trend, and obvious resonance phenomena can be observed (Figure 6c,d). In addition, it can be obviously observed that the values of μ_r are less affected by the change of the raw material content. It is worth noting that the values of μ'' appear negative in the high-frequency region, which indicates that, when the incident wave enters the composite, the electrons in the composite will generate eddy currents under the action of the Lorentz force, thus generating an additional induced magnetic field and radiating electromagnetic energy outward at the high frequency [18]. In addition, it can be observed that the values of tan δ_ε are significantly greater than that of tan δ_μ at the same frequency (Figure 6e,f), which indicates that dielectric loss plays a leading role in the loss process of incident wave.

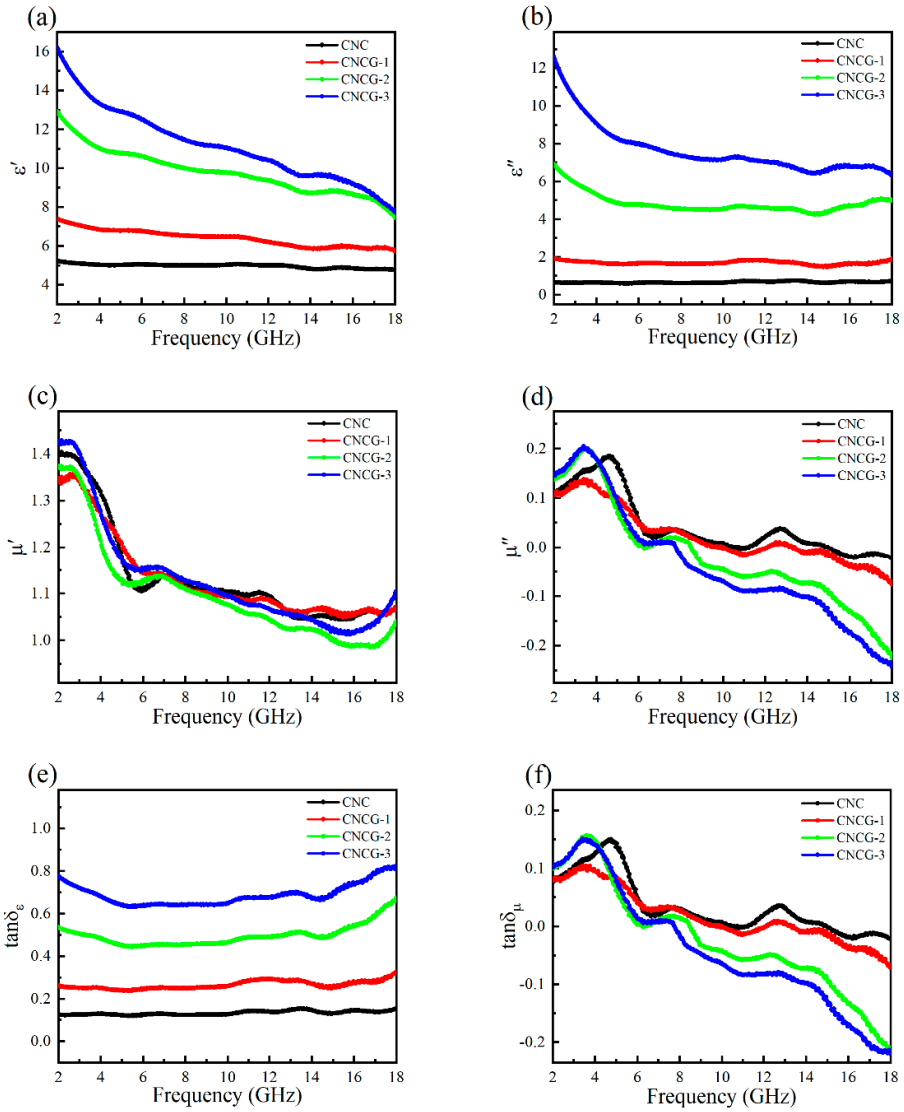

Figure 6. The electromagnetic parameters of all composites. (**a**) The ε' of all composites; (**b**) The ε'' of all composites; (**c**) The μ' of all composites; (**d**) The μ'' of all composites; (**e**) The tan δ_ε of all composites; (**f**) The tan δ_μ of all composites.

According to the transmission line theory, the values of RL in the frequency range of 2–18 GHz were calculated, and then the microwave absorption performances of all composites were evaluated. Generally speaking, when the values of RL are lower than

−10 dB, it means that the incident wave can be effectively absorbed by the composite, and the corresponding frequency range is called the effective absorption bandwidth (EAB). The CNC shows weak microwave absorption performances, and the maximum RL (RL_{max}) is only −5.87 dB (Figure 7a). For CNCG-1, the RL_{max} is −11.70 dB at 12.60 GHz when the thickness is 2.50 mm (Figure 7b). The microwave absorption performances of CNCG-2 are better than that of CNCG-1. The RL_{max} can reach −58.72 dB at the thickness of 1.64 mm. In addition, the RL_{max} can reach −46.79 dB, and the maximum EAB (EAB_{max}) can achieve 5.74 GHz (12.26–18.00 GHz) at the 1.79 mm thickness (Figure 7c). The microwave absorption performances of CNCG-3 are obviously weaker than that of CNCG-2. The RL_{max} can reach −15.96 dB and the EAB_{max} can achieve 5.64 GHz (12.36–18.00 GHz) at the 1.64 mm thickness (Figure 7d). Through the comprehensive analysis of above results, adding appropriate amount of 3D-graphene into the raw materials can effectively improve the microwave absorption performances of the composite.

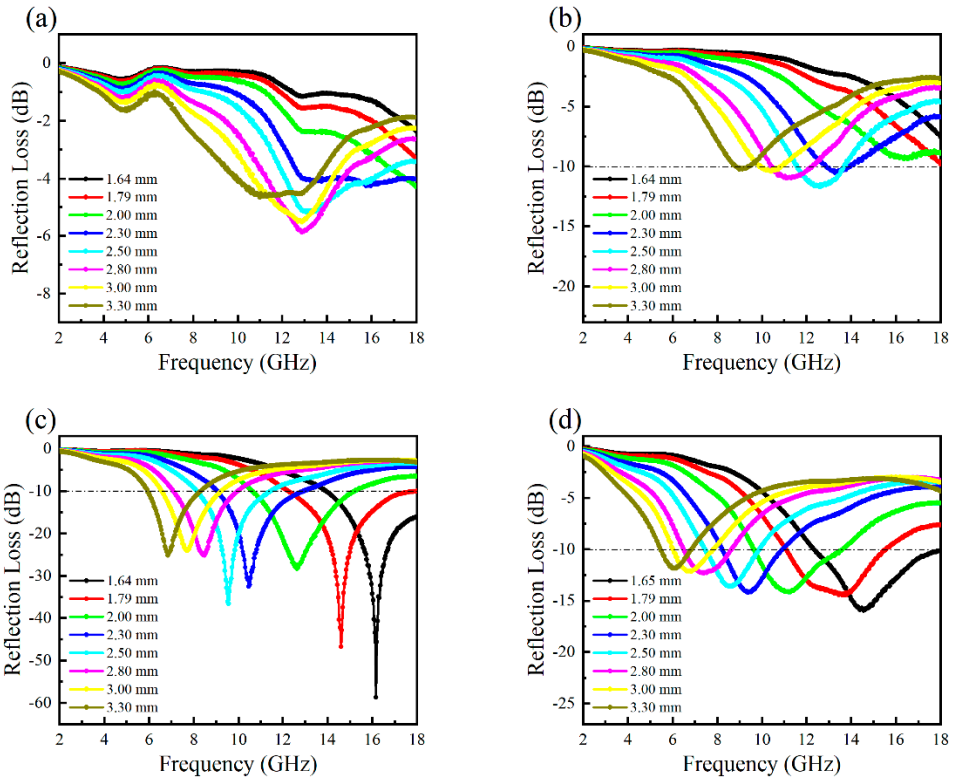

Figure 7. The reflection loss curves of all composites. (**a**) The reflection loss curve of CNC; (**b**) The reflection loss curve of CNCG-1; (**c**) The reflection loss curve of CNCG-2; (**d**) The reflection loss curve of CNCG-3.

The mechanism of dielectric loss can be explained by the Debye theory. The relationship between ε' and ε'' satisfies the following Formula [19]:

$$\left(\varepsilon' - (\varepsilon_s + \varepsilon_\infty)/2\right)^2 + (\varepsilon'')^2 = ((\varepsilon_s - \varepsilon_\infty)/2)^2 \quad (3)$$

where ε_s is the static permittivity in the high frequency limit and ε_∞ is the relative permittivity. The $\varepsilon' - \varepsilon''$ curves of all composites have some semicircles, indicating that there are multiple relaxation processes under the action of incident wave (Figure 8). In addition, it can be clearly seen that, compared with the CNC, the $\varepsilon' - \varepsilon''$ curves of the CNCG present a relatively orderly state. For the CNCG, these relaxation processes are mainly caused by the synergy of interface polarization and dipole polarization [20]. On the one hand, Co particles, the Co-MOF-derived carbon layer, the PVP-K30-derived carbon layer, the 3D-graphene, and the paraffin wax have multiple interfaces with each other, and the charge accumulation at these interfaces causes strong interfacial polarization. On the other hand,

under the action of incident wave, oxygen-containing functional groups, doped nitrogen, and other defects in the composite act as polarization centers to induce a large number of dipoles, which will cause strong dipole polarization. It is noteworthy that straight lines appear at the end of each $\varepsilon' - \varepsilon''$ curve (Figure 8b–d), indicating that conduction loss also plays an important role in the attenuation of incident wave, which is closely related to the properties of carbon in composite [21].

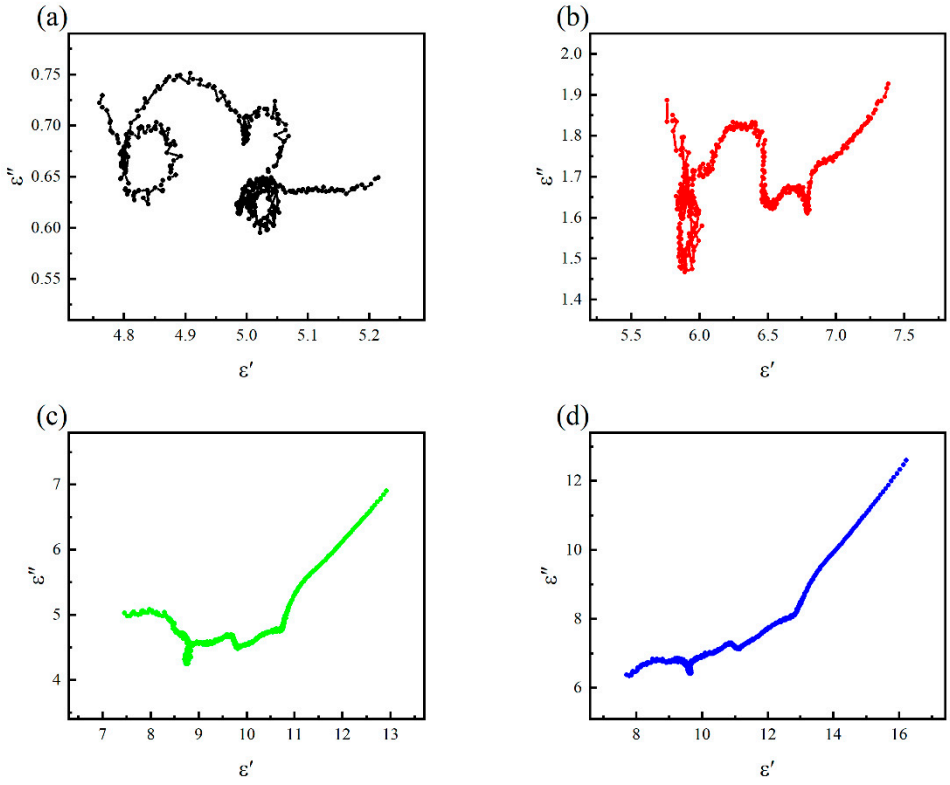

Figure 8. The $\varepsilon' - \varepsilon''$ curves of all composites. (**a**) The $\varepsilon' - \varepsilon''$ curve of CNC; (**b**) The $\varepsilon' - \varepsilon''$ curve of CNCG-1; (**c**) The $\varepsilon' - \varepsilon''$ curve of CNCG-2; (**d**) The $\varepsilon' - \varepsilon''$ curve of CNCG-3.

Magnetic loss is another important mechanism of microwave absorption. In general, magnetic loss is mainly caused by natural resonance, exchange resonance, and eddy current loss. If the eddy current loss is the dominant factor in the magnetic loss over a certain frequency range, the values of C_0 ($C_0 = \mu''(\mu')^{-2}f^{-1}$) remain essentially constant over that frequency range. Conversely, the main factors of magnetic loss are natural resonance and exchange resonance [22]. It can be seen from Figure 9 that the values of C_0 are constantly changing in the frequency range of 2–18 GHz, which indicates that the main factors of magnetic loss of all composites are natural resonance and exchange resonance.

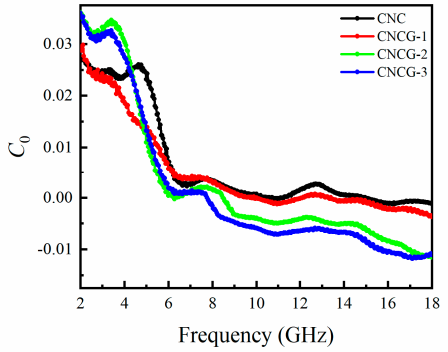

Figure 9. The C_0 curves of all composites.

Microwave attenuation performance is directly determined by two factors: one is the reflection of microwaves on the surface of the material, the other is the absorption of microwaves inside the material. Generally speaking, the former is related to impedance matching ($|Z_{in}/Z_0|$), while the latter is related to attenuation constant (α) [23]. In order to explore the relationship between the microwave absorption performance of the material and α and $|Z_{in}/Z_0|$, the α and $|Z_{in}/Z_0|$ of the CNCG were analyzed in detail. The α can be calculated by the following Formula [24]:

$$\alpha = (\varepsilon''\mu'' - \varepsilon'\mu' + ((\mu''\varepsilon'' - \mu'\varepsilon')^2 + (\mu'\varepsilon'' + \mu''\varepsilon')^2)^{1/2})^{1/2}\sqrt{2}\pi f/c \quad (4)$$

As can be seen from Figure 10a, when the frequency is in the range of 2–18 GHz, the values of α of the CNCG show an increasing trend, and generally follow the order of α (CNCG-3) > α (CNCG-2) > α (CNCG-1). It is worth noting that, although the values of the α of the CNCG-3 are always greater than that of other composites, its microwave absorption performances are relatively weak compared with that of the CNCG-2, mainly due to the limitation of $|Z_{in}/Z_0|$. Good $|Z_{in}/Z_0|$ can ensure that the incident wave enters the material to the maximum extent. When the value of $|Z_{in}/Z_0|$ is equal to 1, it means that the incident wave at this frequency point can completely enter the material [25]. Figure 10b compares the values of $|Z_{in}/Z_0|$ of CNCG at the 1.79 mm thickness. The values of $|Z_{in}/Z_0|$ of the CNCG-2 perform best overall and are significantly better than that of the CNCG-1 and CNCG-3 in the range of 12.00–18.00 GHz, which means that more incident waves can enter the interior of the CNCG-2. Therefore, the excellent microwave absorption performance of the CNCG-2 is the result of the combination of α and $|Z_{in}/Z_0|$.

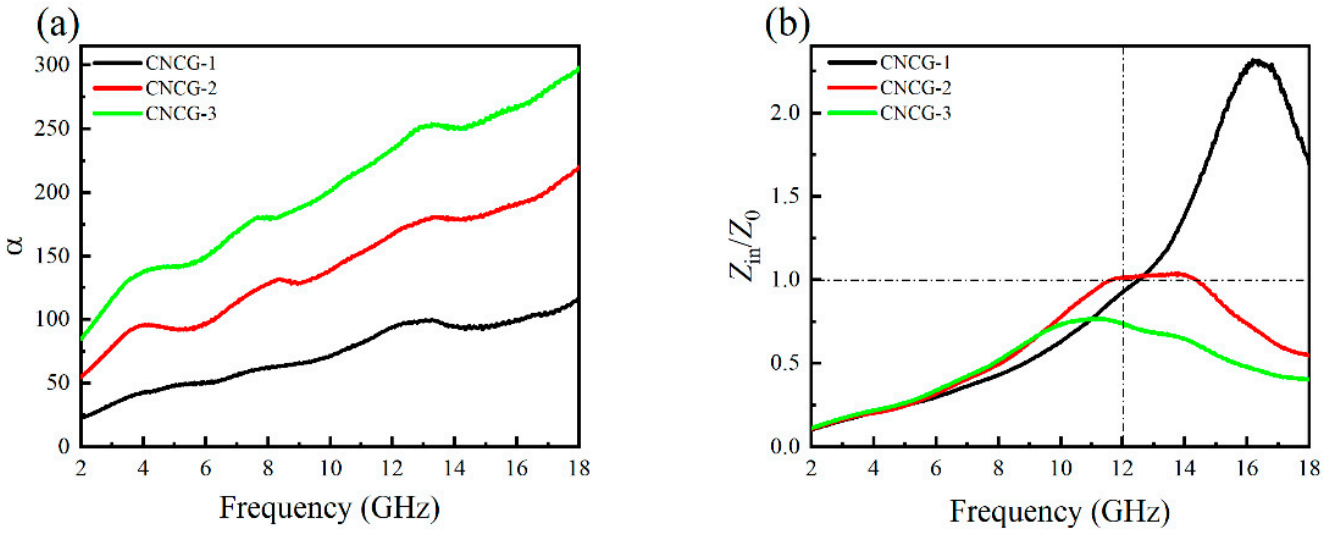

Figure 10. The α curve and $|Z_{in}/Z_0|$ curve of CNCG. (**a**) The α curve of CNCG; (**b**) The $|Z_{in}/Z_0|$ curve of CNCG.

In order to further evaluate the microwave absorption performances of 3D-graphene@C/Co@N-C composite, the microwave absorption performances of other composites are given in Table 1. Through systematic comparison, the 3D-graphene@C/Co@N-C composite has a lower filling rate, a stronger RL_{max}, a wider EAB_{max}, and a thinner thickness, which indicates that the construction of the morphology and spatial structure is a promising strategy to obtain a high-performance microwave absorption composite.

Table 1. Microwave absorption performances of other composites in the previous references.

Materials	Filling Rate (wt%)	RL_{max} (dB)	EAB_{max} (GHz)	Thickness (mm)	Refs.
$Fe_3O_4/NiFe_2O_4/Ni$	60	−58.40	4.90	2.10	[26]
Fe_3O_4@PPy	50	−31.50	5.20	2.50	[27]
CoNi@C	30	−37.50	3.80	2.40	[6]
Co-C@C	25	−58.10	4.56	2.50	[7]
Fe_3O_4@SiO_2@RGO	20	−26.60	4.40	3.00	[28]
3D-graphene@C/Co@N-C	15	−58.72	4.10	1.64	This work
3D-graphene@C/Co@N-C	15	−46.80	5.74	1.79	This work

4. Conclusions

In summary, the 3D-graphene@C/Co@N-C composites were prepared by high-temperature pyrolysis. Under the action of the binder PVP-K30, the 3D-graphene particles can be well decorated on the surface of the CNC after high-temperature pyrolysis. In addition, due to the structural characteristics of the MOFs, the Co particles can be well covered by a carbon layer, which effectively solves the problem of magnetic metal particles being prone to corrosion and oxidation. The microwave absorption performances of all composites can be well adjusted by changing the average dotted density of the 3D-graphene on the CNC. It is worth noting that the RL_{max} can reach −58.72 dB at the thickness of 1.64 mm and the EAB_{max} can achieve 5.74 GHz at the 1.79 mm thickness, which almost covers the whole Ku band. Importantly, the excellent microwave absorption performances can make the 3D-graphene@C/Co@N-C composite become a highly competitive candidate for high-efficiency microwave absorption materials.

Author Contributions: Conceptualization, S.L. and X.T.; methodology, S.L. and X.T.; validation, S.L. and X.T.; formal analysis, S.L. and S.Q.; data curation, S.L. and X.T.; writing—original draft preparation, S.L.; writing—review and editing, S.L. and J.W.; funding acquisition, X.T. and S.L. All authors have read and agreed to the published version of the manuscript.

Funding: This research was funded by the National Science Foundation of China (program no. 21471159) and the Graduate Innovation Practice Fund of Air Force Engineering University (program no. CXJ2021111).

Institutional Review Board Statement: Not applicable.

Informed Consent Statement: Not applicable.

Conflicts of Interest: The authors declare no conflict of interest.

References

1. Gao, S.; Zhang, G.; Wang, Y.; Han, X.; Huang, Y.; Liu, P. MOFs derived magnetic porous carbon microspheres constructed by core-shell Ni@C with high-performance microwave absorption. *J. Mater. Sci. Technol.* **2021**, *88*, 56–65. [CrossRef]
2. Bi, Y.; Ma, M.; Liu, Y.; Tong, Z.; Wang, R.; Chung, K.; Ma, A.; Wu, G.; He, C.; Liu, P.; et al. Microwave absorption enhancement of 2-dimensional CoZn/C@MoS_2@PPy composites derived from metal-organic framework. *J. Colloid Interface Sci.* **2021**, *600*, 209–218. [CrossRef] [PubMed]
3. Liu, T.; Liu, N.; Zhai, S.; Gao, S.; Xiao, Z.; An, Q.; Yang, D. Tailor-made core/shell/shell-like Fe_3O_4@ SiO_2@PPy composites with prominent microwave absorption performance. *J. Alloys Compd.* **2019**, *779*, 831–843. [CrossRef]
4. Wu, F.; Liu, Z.; Xiu, T.; Zhu, B.; Khan, I.; Liu, P.; Zhang, Q.; Zhang, B. Fabrication of ultralight helical porous carbon fibers with CNTs-confined Ni nanoparticles for enhanced microwave absorption. *Compos. Part B* **2021**, *215*, 108814. [CrossRef]
5. Kong, M.; Liu, X.; Jia, Z.; Wang, B.; Wu, X.; Wu, G. Porous magnetic carbon CoFe alloys@ZnO@C composites based on Zn/Co-based bimetallic MOF with efficient electromagnetic wave absorption. *J. Colloid Interface Sci.* **2021**, *604*, 39–51. [CrossRef] [PubMed]
6. Liu, Y.; Chen, Z.; Xie, W.; Qiu, F.; Zhang, Y.; Song, S.; Xiong, C.; Dong, L. Enhanced microwave absorption performance of porous and hollow CoNi@C microspheres with controlled component and morphology. *J. Alloys Compd.* **2019**, *809*, 151837. [CrossRef]
7. Li, S.; Lin, L.; Yao, L.; Zhang, H.; Luo, Q.; Xu, W.; Zhang, C.; Xie, Q.; Wang, L.; Peng, D. MOFs-derived Co-C@C hollow composites with high-performance electromagnetic wave absorption. *J. Alloys Compd.* **2021**, *856*, 158183. [CrossRef]
8. Xu, X.; Ran, F.; Fan, Z.; Cheng, Z.; Lv, T.; Shao, L.; Xie, Z.; Liu, Y. Acidified bimetallic MOFs constructed Co/N co-doped low dimensional hybrid carbon networks for high-efficiency microwave absorption. *Carbon* **2021**, *171*, 211–220. [CrossRef]

9. Song, S.; Zhang, A.; Chen, L.; Jia, Q.; Zhou, C.; Liu, J.; Wang, X. A novel multi-cavity structured MOF derivative/porous graphene hybrid for high performance microwave absorption. *Carbon* **2021**, *176*, 279–289. [CrossRef]
10. Qiu, Y.; Yang, H.; Ma, L.; Lin, Y.; Zong, H.; Wen, B.; Bai, X.; Wang, M. In situ-derived carbon nanotube-decorated nitrogen-doped carbon-coated nickel hybrids from MOF/melamine for efficient electromagnetic wave absorption. *J. Colloid Interface Sci.* **2021**, *581*, 783–793. [CrossRef]
11. Jia, Z.; Kong, M.; Yu, B.; Ma, Y.; Pan, J.; Wu, G. Tunable Co/ZnO/C@MWCNTs based on carbon nanotube-coated MOF with excellent microwave absorption properties. *J. Mater. Sci. Technol.* **2022**, *127*, 153–163. [CrossRef]
12. Li, S.; Yang, K.; Ye, P.; Ma, K.; Zhang, Z.; Huang, Q. Three-dimensional porous carbon/Co_3O_4 composites derived from graphene/Co-MOF for high performance supercapacitor electrodes. *Appl. Surf. Sci.* **2020**, *503*, 144090. [CrossRef]
13. Huang, Z.; Liang, R.; Zhang, B.; He, Y.; Kim, J. Evolution of flexible 3D graphene oxide/carbon nanotube/polyaniline composite papers and their supercapacitive performance. *Compos. Sci. Technol.* **2013**, *88*, 126–133. [CrossRef]
14. Maleki-Ghaleh, H.; Siadati, M.; Fallah, A.; Zarrabi, A.; Afghah, F.; Koc, B.; Abdolahinia, E.; Omidi, Y.; Barar, J.; Akbari-Fakhrabadi, A.; et al. Effect of zinc-doped hydroxyapatite/graphene nanocomposite on the physicochemical properties and osteogenesis differentiation of 3D-printed polycaprolactone scaffolds for bone tissue engineering. *Chem. Eng. J.* **2021**, *426*, 131321. [CrossRef]
15. Kogularasu, S.; Govindasamy, M.; Chen, S.; Akilarasan, M.; Mani, V. 3D graphene oxide-cobalt oxide polyhedrons for highly sensitive non-enzymatic electrochemical determination of hydrogen peroxide. *Sens. Actuators B* **2017**, *253*, 773–783. [CrossRef]
16. Shen, Y.; Zhang, F.; Song, P.; Zhang, Y.; Zhang, T.; Wen, X.; Ma, J.; Zhang, D.; Du, X. Design and synthesis of magnetic porous carbon nanofibers with excellent microwave absorption. *J. Alloys Compd.* **2022**, *903*, 163971. [CrossRef]
17. Liang, L.; Li, Q.; Yan, X.; Feng, Y.; Wang, Y.; Zhang, H.; Zhou, X.; Liu, C.; Shen, C.; Xie, X. Multifunctional magnetic $Ti_3C_2T_x$ MXene/graphene aerogel with superior electromagnetic wave absorption performance. *ACS Nano* **2021**, *15*, 6622–6632. [CrossRef]
18. Guan, H.; Wang, H.; Zhang, Y.; Dong, C.; Chen, G.; Wang, Y.; Xie, J. Microwave absorption performance of $Ni(OH)_2$ decorating biomass carbon composites from Jackfruit peel. *Appl. Surf. Sci.* **2018**, *447*, 261–268. [CrossRef]
19. Meng, X.; Lei, W.; Yang, W.; Liu, Y.; Yu, Y. Fe_3O_4 nanoparticles coated with ultra-thin carbon layer for polarization-controlled microwave absorption performance. *J. Colloid Interface Sci.* **2021**, *600*, 382–389. [CrossRef]
20. Zhang, Z.; Zhao, Y.; Li, Z.; Zhang, L.; Liu, Z.; Long, Z.; Li, Y.; Liu, Y.; Fan, R.; Sun, K.; et al. Synthesis of carbon/SiO_2 core-sheath nanofibers with Co-Fe nanoparticles embedded in via electrospinning for high-performance microwave absorption. *Adv. Compos. Hybrid Mater.* **2022**, *5*, 513–524. [CrossRef]
21. Li, W.; Zhang, Z.; Lv, Y.; Wu, Z.; Yang, L.; Zou, W.; Zou, Y. Ultralight Coral-like hierarchical Fe/CNTs/Porous carbon composite derived from biomass with tunable microwave absorption performance. *Appl. Surf. Sci.* **2022**, *571*, 151349. [CrossRef]
22. Xu, X.; Ran, F.; Fan, Z.; Lai, H.; Cheng, Z.; Lv, T.; Shao, L.; Liu, Y. Cactus-inspired bimetallic metal-organic framework-derived 1D-2D hierarchical Co/N-decorated carbon architecture toward enhanced electromagnetic wave absorbing performance. *ACS Appl. Mater. Interfaces* **2019**, *11*, 13564–13573. [CrossRef] [PubMed]
23. Ma, M.; Bi, Y.; Jiao, Z.; Yue, J.; Liao, Z.; Wang, Y.; Ma, Y.; Huang, W. Facile fabrication of metal–organic framework derived Fe/Fe3O4/FeN/N-doped carbon composites coated with PPy for superior microwave absorption. *J. Colloid Interface Sci.* **2022**, *608*, 525–535. [CrossRef] [PubMed]
24. Zhang, P.; Zhang, X.; Li, B.; Xu, L.; Dang, F.; Li, B. Enhanced microwave absorption performance in an ultralight porous single-atom Co-N-C absorber. *Adv. Compos. Hybrid Mater.* **2021**, *4*, 1292–1301. [CrossRef]
25. Ma, M.; Li, W.; Tong, Z.; Yang, Y.; Ma, Y.; Cui, Z.; Wang, R.; Yu, P.; Huang, W. 1D flower-like Fe_3O_4@SiO_2@MnO_2 nanochains inducing RGO self-assembly into aerogels for high-efficient microwave absorption. *Mater. Des.* **2020**, *188*, 108462. [CrossRef]
26. Li, Y.; Wu, K.; Jin, K.; Qian, Y.; Qian, N.; Jiang, K.; Wu, W.; Tong, G. Controllable synthesis and enhanced microwave absorbing properties of Fe_3O_4/$NiFe_2O_4$/Ni heterostructure porous rods. *Appl. Surf. Sci.* **2016**, *387*, 190–201. [CrossRef]
27. Qiao, M.; Lei, X.; Ma, Y.; Tian, L.; Su, K.; Zhang, Q. Well-defined core-shell Fe_3O_4@polypyrrole composite microspheres with tunable shell thickness: Synthesis and their superior microwave absorption performance in the Ku band. *Ind. Eng. Chem. Res.* **2016**, *55*, 6263–6275. [CrossRef]
28. Liu, L.; He, N.; Wu, T.; Hu, P.; Tong, G. Co/C/Fe/C hierarchical flowers with strawberry-like surface as surface plasmon for enhanced permittivity, permeability, and microwave absorption properties. *Chem. Eng. J.* **2019**, *355*, 103–108. [CrossRef]